Experimental and Discrete Element Method Analysis of Galvanized Steel Scrap Particles Along and After an Inclined Chute

Georgakopoulos, Evangelos; Hosseini, Ashkan; Kerry, Timothy; Hage, Johannes; Meijer, Koen; Offerman, Erik; Yang, Yongxiang

DOI
10.1002/srin.202200075

Publication date
2022

Document Version
Final published version

Published in
Steel Research International

steel research international
www.steel-research.de

Experimental and Discrete Element Method Analysis of Galvanized Steel Scrap Particles Along and After an Inclined Chute

Evangelos Georgakopoulos, Ashkan Hosseini, Timothy Kerry, Johannes Hage, Koen Meijer, Erik Offerman, and Yongxiang Yang*

HIsarna is a novel ironmaking process with great raw materials versatility that is attractive for various secondary resources. Among the materials that can be recycled, there is steel scrap which is fed to the furnace bath through an inclined chute. The velocity distribution of the scrap particles along the chute affects the particles' distribution on the liquid slag and, thereupon, the efficient operation of the reactor. In this study, the flow of steel scrap particles along an inclined chute with the same dimensions as those of the actual chute of the HIsarna plant is investigated experimentally and numerically. The simulations are validated using chute tip velocity and mass fractions collected at the different compartments of a sampling device. Translational and angular velocity distributions along and across the chute are reported, and the effect of different parameters are investigated. The impact of the shape of the particles on the simulation process is found to be negligible. The angular velocity distribution in cross-sections of the chute exhibited a V-shaped orientation, whereas the translational velocity displayed similar values across the cross-sections. Moreover, translational velocity appeared to increase with increasing inclination angles, whereas angular velocity increased with decreasing batch size.

1. Introduction

Granular materials are widely encountered in numerous physical occasions and engineering applications. The understanding of their flow behavior on inclined surfaces is considered to be of high significance for the description and forecast of several geophysical[1–6] phenomena like landslides, sand flows, debris flows or avalanches, and industrial processes[7–14] such as the storage, handling, and transportation of materials like cereals, seeds, minerals, or pharmaceutical powders.

Particularly in the metallurgical industry granular materials and their handling hold an important role. The scrap metal feeding chute of the HIsarna furnace is such an example. The HIsarna process is a novel ironmaking process owned by Tata steel that shows great potential for the recycling of Zn-bearing wastes. A pilot-scale facility of this technology is operating at the Tata steel site in Ijmuiden, Netherlands, since 2010. The HIsarna process is a combination of two different technologies, a cyclone converter furnace (CCF) at the top and a smelting reduction vessel (SRV) at the bottom. Plant operation has shown that the furnace is characterized by a high raw materials versatility and is therefore attractive for processing secondary iron sources. Among the materials that can be recycled through HIsarna is galvanized steel scrap. This type of material directly enters the SRV part of the furnace in a batch-wise manner. The feeding system in this case is an inclined chute. The distribution of the material on the burden surface of the SRV is crucial for the efficient operation of the furnace since it appears to significantly affect the thermal conditions of the bath. The flow behavior of the feeding material in the chute and its velocity at the tip of the chute are factors that significantly affect the distribution of the scrap on the burden surface. Thus, a better understanding of the phenomena occurring during the flow of the scrap along the chute is required.

Due to its practical importance in several industrial applications, the flow of granular materials along an inclined chute has been studied by several researchers. Augenstein and Hogg[7] performed an experimental study on the sand flow behavior on inclined surfaces. Under different surface inclination, particle size, and surface roughness, the velocity profile is measured. By distinguishing the total stream into different streamlines at constant fractions of the total bed depth, they found that regardless of the tested surface friction, the velocity is distributed differently with material bed depth. The layers of particles adjacent to or in direct touch with the surface had notably lower velocities compared to those of the free surface of the flowing stream. Ishida and Shirai[8] studied the flow of

E. Georgakopoulos, A. Hosseini, T. Kerry, E. Offerman, Y. Yang
Department of Materials Science and Engineering
Delft University of Technology
2628 CN Delft, Netherlands
E-mail: a.hosseini-1@tudelft.nl

J. Hage, K. Meijer
R&D Ironmaking
Tata steel IJmuiden
1951 JZ Velsen-Noord, Netherlands

The ORCID identification number(s) for the author(s) of this article can be found under https://doi.org/10.1002/srin.202200075.

DOI: 10.1002/srin.202200075

three types of particles (i.e., glass beads, porous alumina, and fluidized catalytic cracking) down an inclined open chute of which the bottom was rough and found that the velocity distribution near the bottom plate was linear. Moreover, it was found that the velocity gradient in that region was almost independent of the thickness of the particles layer but highly dependent on the slope of the chute, with steeper slopes increasing the velocity gradient. Jop et al.[15] studied the flow of glass beads along an inclined rectangular chute and reported 3D velocity profiles estimated based on a proposed frictional law of granular materials. Bi et al.[16] investigated the influence of bottom roughness on monodisperse disks flowing down an inclined chute using a high-speed camera. According to their findings, when steady fully developed granular flows occur, the mean discharge velocity is proportional to the flow depth. Shirsath et al.[17] studied the flow behavior of spherical glass particles of uniform size. The particles were flowing on an affixed angle rotating rectangular chute. They concluded that the flow acceleration (by centrifuge force) is diminished by Coriolis force.

A better and more detailed insight into granular flows has been achieved when experimental results were combined with numerical simulations. The discrete element method (DEM) is a feasible numerical method widely applied to describe the motion of granular and discontinuous materials. More particularly, DEM has been extensively used to describe granular flows in several industrial applications, like in fluidized beds,[18–20] drum mixers,[21,22] hoppers charging and discharging systems,[23–27] and inclined chutes.[14,28–32] Especially for the flow along inclined chutes, Mio et al.[31] modeled the behavior of spherical sinter particles to calculate the velocity and size segregation of particles along the chute. They have reported that velocity is decreased with rolling friction increased. Yu and Saxen[14] have simulated the flow of spherical particles being discharged from a hopper to a static chute using the DEM approach validated by experimental data. According to their findings, the average velocity for the bulk of the material flow at the tip of the chute only depends on the angle of the chute whereas the angular and translational velocity distributions of the flow become more uniform as the flow approaches the tip of the chute. Yu and Saxen[32] have investigated the effect of particle shape on velocity distribution and size segregation. To fulfill that, they have developed a DEM model and validated it with experimental data. More particularly, the authors described the flow of ternary-size pellets and coke along and after an inclined fixed chute. They have also reported that the shape of the particle was not found to affect the trajectory of the particles after leaving the chute and only appeared to influence the angular velocity of the flowing particles.

In this article, the flow behavior of steel scrap particles along a continuously inclined chute is studied both experimentally and numerically. In particular, the effects of particles shape and size, batch size, and dosing chute inclination angle on the velocity of the flowing material and its trajectory after leaving the chute are investigated.

2. Experimental Section

2.1. Experimental Study

For the experimental investigation of the behavior of steel scrap particles flowing down the chute, a laboratory-scale chute made of Plexiglas was used as shown in **Figure 1**. For the needs of the study, only the bottom part of the chute was used. This part of the apparatus hosts a pneumatically driven valve opening at a constant velocity of $1\,\mathrm{m\,s^{-1}}$ and the final inclined part of the chute. The scale used for the bottom part of the apparatus was the same as that of the actual corresponding part of the dosing chute used for the HIsarna furnace. In particular, the inner diameter of the experimental chute was 140 mm and the length of its inclined part was 500 mm. By interchanging the bottom part of the chute different inclination angles could be tested. In particular, inclination angles of 20°, 25°, 30°, 35°, and 40° to the vertical were examined.

The investigated types of galvanized steel scrap are presented in Figure 1C. Based on their shape, the particles have been distinguished into three categories, namely "compacted scrap," "music notes," and "coupons."

For each type of steel scrap particle investigated, 3 different batch sizes (1, 2, and 3 kg) were tested. The tested batch of particles was first placed above the closed valve. After the opening of the valve, the material was left to flow along the inclined part of the chute and the flow was captured at 1000 fps, using the Phantom Miro M310 high-speed camera. From the analysis of the acquired videos, it was possible to estimate the velocity of individual particles of the flow at the exit section of the chute. In particular, the particles velocity was approximated using Equation 1

$$v = \frac{L}{N_\mathrm{f}\Delta t} \tag{1}$$

where L is the length of the exiting portion of the chute, N_f is the number of frames required for the particle to travel the distance L, and Δt is the time interval between consecutive frames ($\Delta t = 1/1000$ s).

For each flow, the velocity of a number of particles entering the exit zone after similar time intervals up until the whole flow has left the chute, was estimated. The velocity of the whole flow was the average value of these velocities.

Particles leaving the chute will be collected in a sampling box (Plexiglas material). The box was divided into 9 different slots with identical dimensions (**Figure 2**). For each run, the collected mass at each slot was collected and weighted to calculate the mass fractions.

2.2. DEM Theory

DEM is used to model the granular flow of scrap particles. Each particle has 6° of motion and 2 types of motion, translational and rotational which are described through Newton's second law of motion.[33]

$$m_i \frac{\mathrm{d}v_i}{\mathrm{d}t} = \sum_{j=1}^{K} (F_{n,ij} + F_{n,ij}^{\mathrm{d}} + F_{\mathrm{t},ij} + F_{t,ij}^{d}) + m_i g \tag{2}$$

$$I_i \frac{\mathrm{d}\omega_i}{\mathrm{d}t} = \sum_{j=1}^{K} (T_{\mathrm{t},ij} + T_{\mathrm{r},ij}) \tag{3}$$

Soft sphere approach was used to calculate the forces in the aforementioned equations. In this approach, particles can be

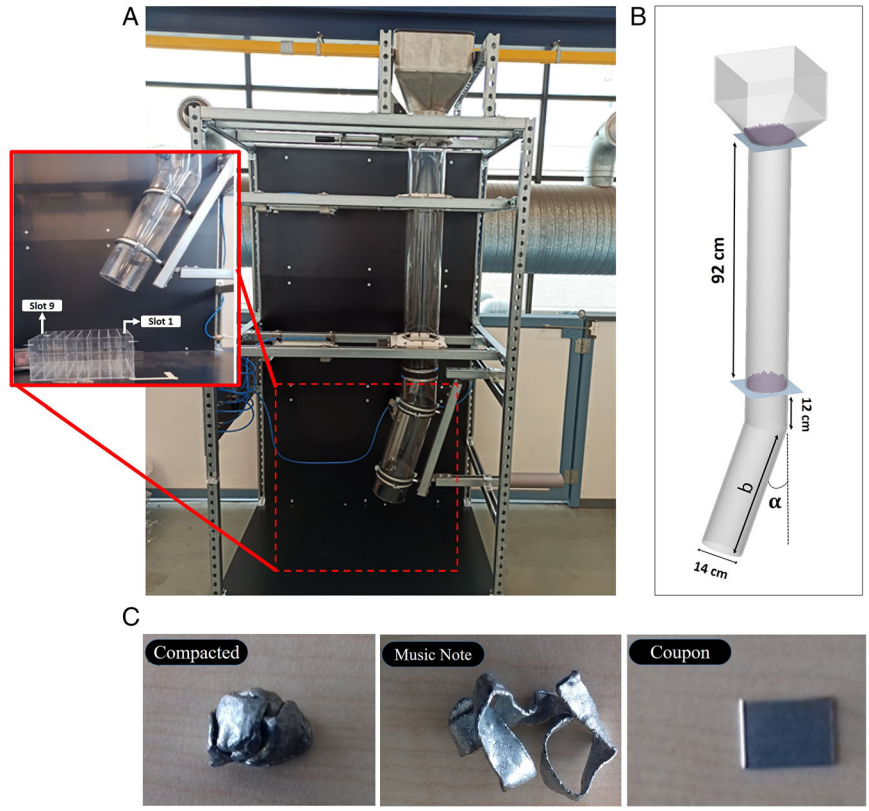

Figure 1. A) The laboratory-scale chute; B) the bottom part of the chute with the sampling box and C) different types of steel scrap particles.

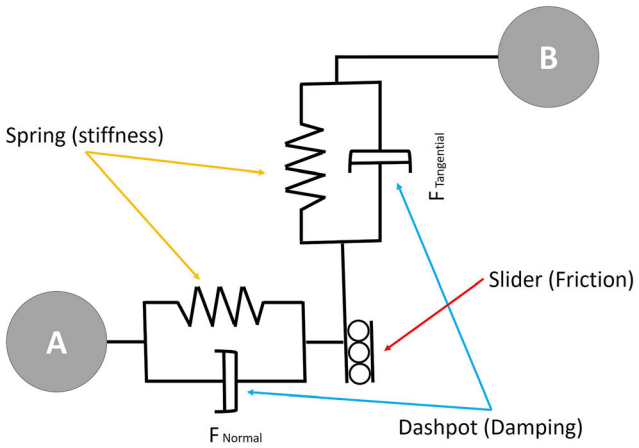

Figure 2. Schematic view of spring and dashpot for contact force modeling.

overlapped in both normal and tangential directions on which directional forces depend.

To consider the elastic and plastic nature of particles, the contact model composed of spring and dashpot in the normal direction and an extra slider in the tangential direction was considered as shown in Figure 2. Different contact models based on this approach are available[4,24,34–51] and in this study Hertz–Mindlin model with relative velocity dependent (RVD) Rolling Friction was used.

F_n the normal force, is a function of normal overlap and is given by

$$F_{n,ij} = \frac{4}{3} E^* \sqrt{R^*}.\delta_n^{1.5} \tag{4}$$

$$E^* = \frac{1}{(1-\vartheta_i^2/E_i) + (1-\vartheta_j^2/E_j)} \tag{5}$$

$$R^* = R_i R_j/(R_i + R_j) \tag{6}$$

Additionally, there is a normal damping force given by

$$F_{n,ij}^{\mathrm{d}} = -2\sqrt{\frac{5}{6}}.\beta\sqrt{S_n m^*}.v_{n,ij}^{\mathrm{rel}} \tag{7}$$

where m^*, β, and S_n are defined as follows

$$m^* = \left(\frac{1}{m_i} + \frac{1}{m_j}\right)^{-1} \tag{8}$$

$$\beta = \frac{lne}{\sqrt{ln^2 e + \pi^2}} \tag{9}$$

$$S_n = 2.E^* \sqrt{\delta_n R^*} \tag{10}$$

The tangential force, F_t is calculated using the following expression

$$F_{t,ij} = -\delta_t S_t \tag{11}$$

$$S_t = 8G^* \sqrt{\delta_n R^*} \tag{12}$$

In tangential direction, there will be a damping force defined as

$$F^d_{t,ij} = -2\sqrt{\frac{5}{6}}\beta\sqrt{S_t m^*}v^{rel}_{t,ij} \tag{13}$$

The torque is of two types, one is caused by tangential forces and the other arises when the rolling friction between particles and surface is noticeable.

The tangential torque is defined as

$$T_{ij} = R_i(F^d_{t,ij} + F_{t,ij}) \tag{14}$$

To calculate the torque related to rolling friction, RVD approach[52] is used. In this approach, the instantaneous rotational velocity of two particles that are in touch are used to calculate the relative rotational velocity, and ultimately it is used in the following expression to calculate the torque

$$T_{r,ij} = -\mu_r F_{n,ij} R^* \widehat{\omega}_{rel,ij} \tag{15}$$

$$\widehat{\omega}_{rel,ij} = \widehat{n}_{ij} \times v_{t,ij}/|v_{t,ij}| \tag{16}$$

$$v_{t,ij} = \begin{cases} -\frac{1}{2}(\omega_i + \omega_j) \times \vec{r}_{ij}, & \text{particle} - \text{particle contacts} \\ -R_i\omega_i \times \widehat{n}_{ij}, & \text{particle} - \text{geometry contacts} \end{cases} \tag{17}$$

Here $\widehat{n}_{ij}$ is a unit vector pointing from particle i to the point of contact, and r_{ij} is center to canter distance of overlapped particles.

At each time step, all forces and torques will be calculated for individual particles and by solving Equation (1) and (2), by an explicit method, the particle positions are updated.[33]

2.3. Modeling Procedure

The model in this study was developed for compacted scrap using EDEM software, which is a commercial discrete element method solver. Similar to the experimental process, the simulated batch of particles was injected above the closed valve where they were allowed to settle under gravity. After the formation of a stable bed, the valve (which was simulated as a simple rectangular plate) opened rapidly (at 1 m s^{-1}) and the batch of particles was left to flow along the chute to fall into the sampling box.

To develop the model, information regarding particle size distribution and particle shape is necessary. Scrap particles, in compact form, vary drastically in shape and size, however, most of the particles are highly compacted and close to spherical shapes.

Table 1. Particle classification and size calculations for spherical approach.

Size class	Equivalent spherical diameter [cm]	Number of particles (for 1 kg sample)	Mass fraction	Existing shape class
A	0.6354	210	0.2	All
B	0.704	52	0.07	Long
C	0.7854	65	0.13	Oval - rectangular - triangle - irregular
D	0.9779	71	0.25	Oval - rectangular - triangle - irregular
E	1.2797	22	0.19	Oval - rectangular - triangular
F	1.661	7	0.13	Oval - rectangular - triangular
Total Batch	0.8344	427	1	

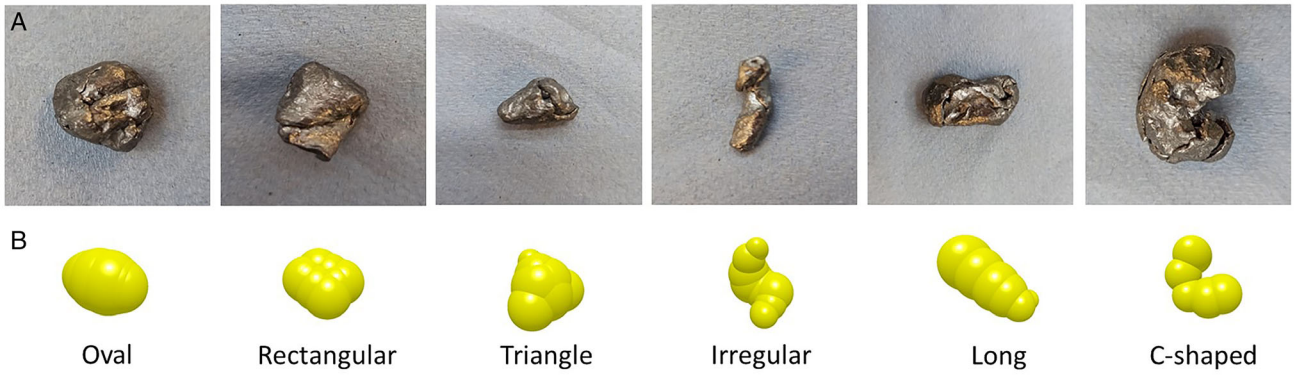

Figure 3. A) Representative shapes of actual steel scrap particles and B) Representations by spherical assembled particles in the discrete element method (DEM) simulations.

Table 2. Material properties for Plexiglas and steel particles used in simulations.

Steel Particles		
Density	7800	Kg m^{-3}
Poisson ratio	0.25	
Shear modulus	7.60 E + 10	Pa
Particle–particle static friction coefficient	0.4	
Particle–particle rolling friction coefficient	0.05	
Particle–particle restitution coefficient	0.6	
Plexiglas		
Density	1200	Kg m^{-3}
Poisson ratio	0.4	
Shear modulus	8.93 E + 08	Pa
Particle versus Plexiglas static friction coefficient	0.3	
Particle versus Plexiglas rolling friction coefficient	0.05	
Particle versus Plexiglas restitution coefficient	0.5	

To include the particle size distribution, one kilogram of scrap sample was taken from the plant and particles are divided into six "Size Classes" based on the similarities in particles' approximate dimension (particle size). Each size group contains particles with the same particle size but various particle shapes.

Using classified particles, it is possible to consider two approaches for particle modeling.

In the first approach, the effect of the actual shapes of the particles was considered negligible and all the particles were considered spherical (spheric model). From the number of particles that belong to each category and the average particle mass describing each group, the equivalent spherical diameter was calculated and reported in **Table 1**. In all the simulated cases, the number of particles composing every batch size tested was the same as in the corresponding experimental trials.

In the second approach, the actual shapes of the steel scrap particles were taken into account (shaped model) by considering 6 different shape classes which are frequently appearing inside the batch sample shown in **Figure 3**A.

Based on the experimental measurements, large particles displayed limited variety in particles shape but wider shape variations are observed for smaller classes. For example in size class A, all of the shape classes are observed while for size class F only oval, rectangular and triangle shape classes exist. The result of this observation is reported in the last column of Table 1.

The real shape of particles are approximated based on the multiple overlapping spheres forming a cluster close to the real shapes (Figure 3B) and different shapes are incorporated into each size class with an equal mass ratio for each existing shape class.

For both approaches, the material properties and interaction coefficients listed in **Table 2** are used to set up the model. The physical properties of steel and Plexiglas are taken from the EDEM software database and interaction coefficients are obtained through the "guessing" procedure in a valid interval for each coefficient. In this procedure, which has been used in other DEM studies,[53–55] an initial guess of interaction values are chosen and then tuned to obtain output parameters that are matched with their counterpart experimental measures. In this study, the chosen initial values are based on the study of Yu and Saxen,[14] for spherical steel particles and Plexiglas surface interaction. Using initial values for all interaction parameters, simulations are performed and tip velocity and mass fraction in the sampling box are obtained and compared with experimental data. This procedure is repeated until the best match for tip velocity and mass fraction using tuned interaction coefficients are obtained.

In general, the available coefficients in the literature are usually referring to spherical particles of a relatively large or

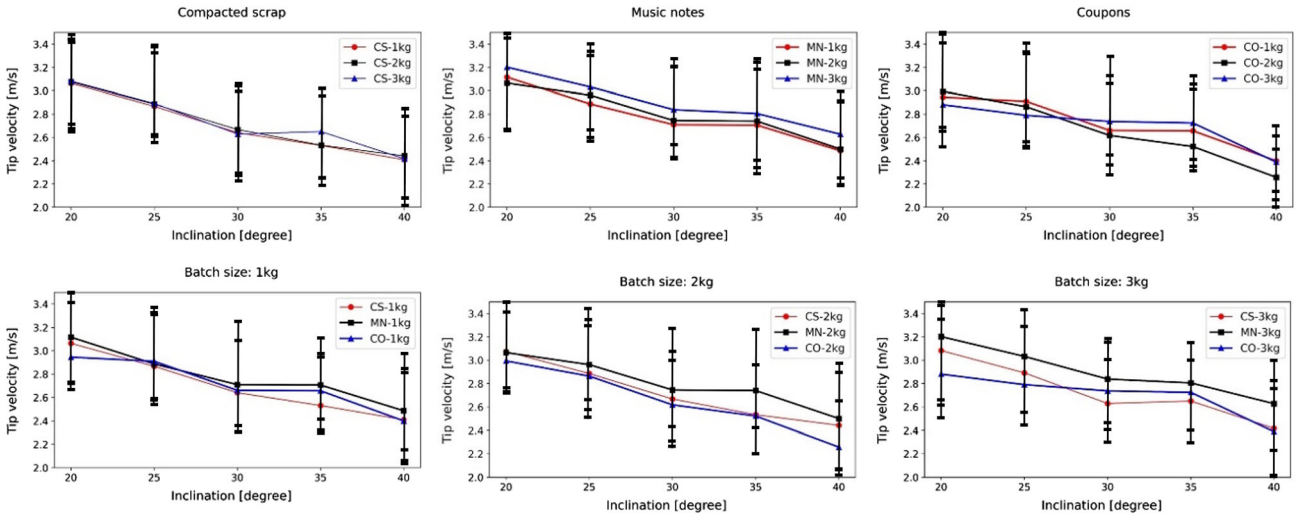

Figure 4. Tip velocities of the flowing steel scrap as a function of scrap shape, batch size, and angle of inclination (CS: Compact Scrap, MN: Music Note, CO: coupons).

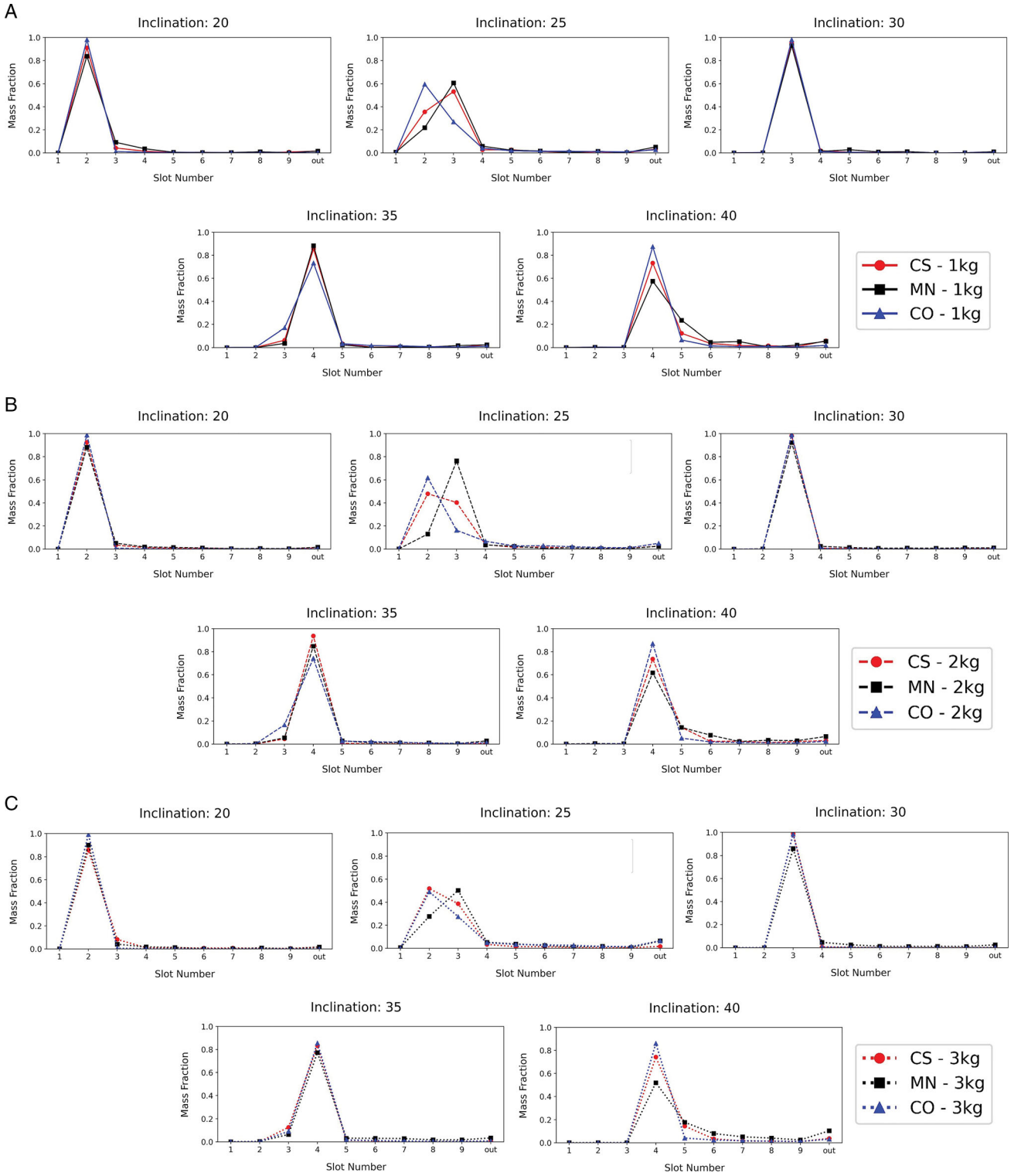

Figure 5. Mass distribution of the flowing particles as a function of scrap shape, and angle of inclination for a batch size of: A) 1 kg, B) 2 kg, and C) 3 kg (CS: Compact Scrap, MN: Music Note, CO: coupons).

moderate size (above 1 cm in diameter). However, size and shape can have a noticeable effect on the interaction coefficients. For example, spherical particles with relatively large size (5 to 10 mm in diameter) might have a higher coefficient of restitution than smaller particles. Also, irregular-shaped particles have a rather lower coefficient of restitution compared to

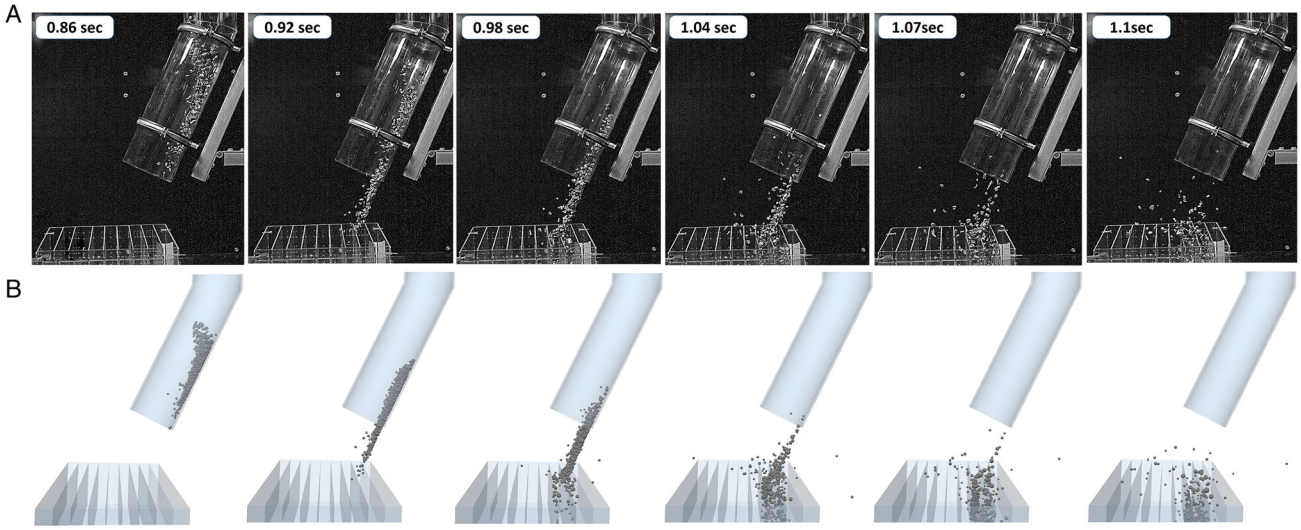

Figure 6. Comparison of snapshots of particle flow and trajectories along and after leaving the chute between: A) experiments and B) DEM simulations for inclination of 20° and batch size of 1 kg.

spherical ones (of the same size) and often come to rest after one or two bounces on a surface. Similarly, the friction coefficient of spherical particles is lower than that of particles with irregular shapes. So in the current case, interaction parameter tuning is necessary due to the wide variety in size and shape of steel scrap particles.

Finally, the simulations were conducted using Euler time integration with a time step of 10^{-6} s and domain cells size equal to 3 times of particle minimum radius.

3. Results and Discussion

3.1. Experimental Results

The velocity of the material leaving the chute tip is a determining factor for the distribution of the material on the burden surface of the furnace. The average exit velocities of the tested steel scrap flow as a function of the tested shapes of scrap and batch sizes are presented in **Figure 4**. According to the results, it is clear that neither the shape of the material nor the size of the batch appears to significantly affect the velocity at which the flows exit the chute. In contrast, the angle at which the chute is inclined notably influences the velocity of the material with increasing angles resulting in lower exit velocities.

The error bars of the graphs represent the deviation of the velocities estimated for each one of the tracked particles from the average tip velocity of the flow. According to them, an average deviation of ≈10% is indicated. This noticeable deviation should be ascribed to the higher velocities recorded for the particles at the front part of the flow compared to those at the rear part of it. In other words, a longitudinal velocity gradient is observed at the investigated part of the chute.

The trajectory of steel scrap after leaving the dosing chute is also of high importance for the efficient operation of the furnace. An estimation of the trajectories of the flowing particles after leaving the chute was attempted by using a sampling box. In **Figure 5**, the fractions of the tested batches collected in the different compartments of the sampling device are presented.

From the graphs, it is clear that in most of the tested cases, the mass distribution of the tested particles was considerably narrow, with the great majority of them falling in only one compartment. Both the shape of the scrap particles and the size of the tested batch did not appear to affect the trajectory of the falling material and only the angle of inclination appeared to significantly influence it with higher angles resulting in particles traveling greater distances and falling in compartments with higher numbers. Only in the case of 25° of inclination, the mass distribution of the tested material was different. In particular, when the chute was inclined at 25°, the distribution of the material was broader falling in two different compartments, with the greater fraction of compacted scrap and coupons falling in compartment 2 and that of music notes falling in compartment 3. The particular behavior was explained after carefully examining the recording of the particular case. In fact, it is the position of the box at the particular angle of inclination that causes this discrepancy in the mass distribution of the material in the sampling box (**Figure 5**). More particularly, the flow of the material hits the wall separating compartment numbers 2 and 3 and based on the shape of the material and the batch size tested, the particles fall in the different compartments.

According to the results, the distribution of the particles is not particularly wide, with the great majority of them falling in only one slot regardless of their size or the batch size tested. Only in the case of 40°, the particles displayed a wider distribution, with a notable amount of particles of all sizes falling to more than one compartment.

3.2. Model Validation

From the experimental results, it is clear that steel scrap shape does not have a notable effect on either the exit velocity of the flowing particles or their trajectory after leaving the chute.

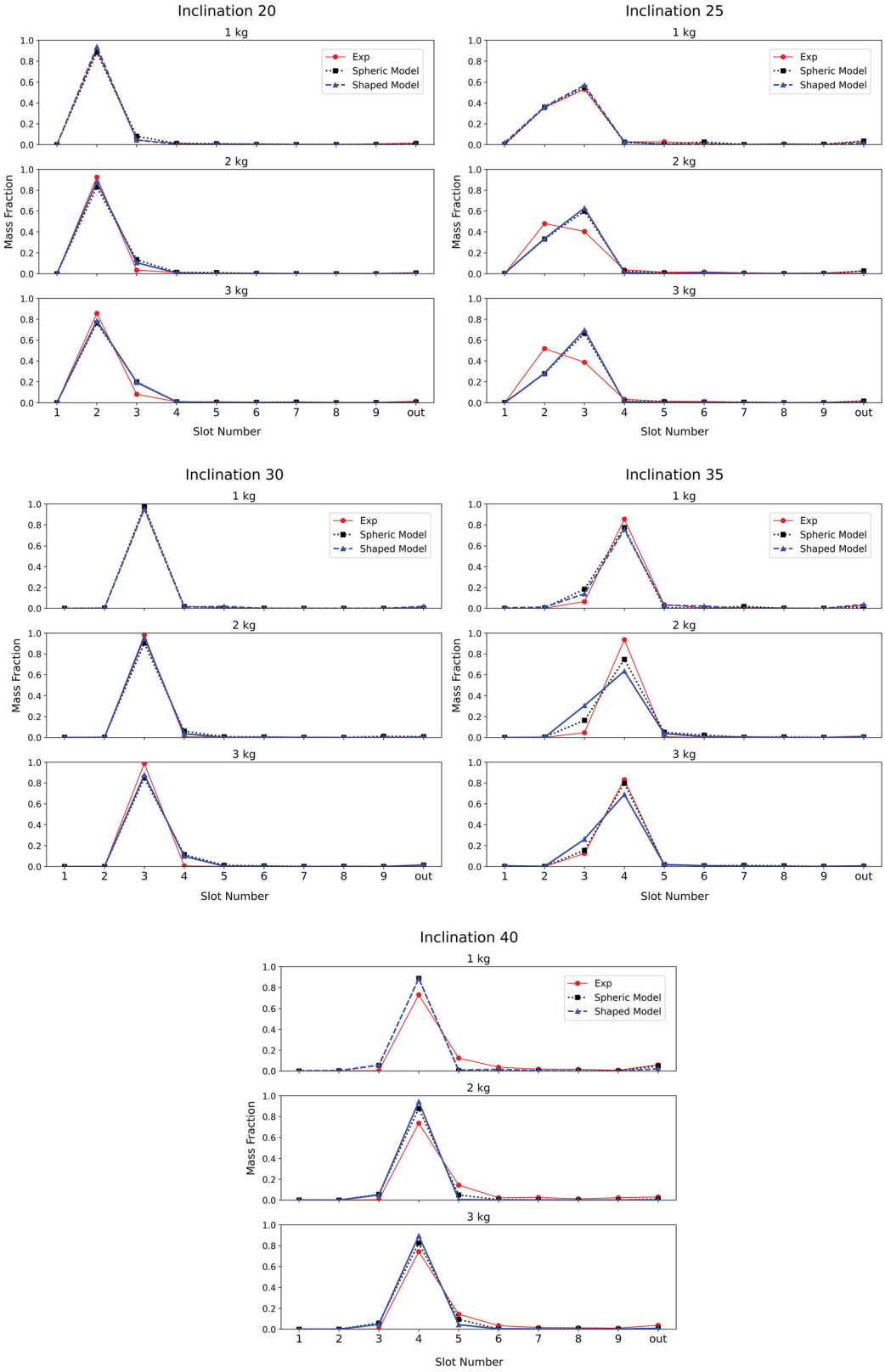

Figure 7. Mass fraction distributions of compacted steel scrap particles as they have been determined experimentally and by DEM simulations using both modeling scenarios.

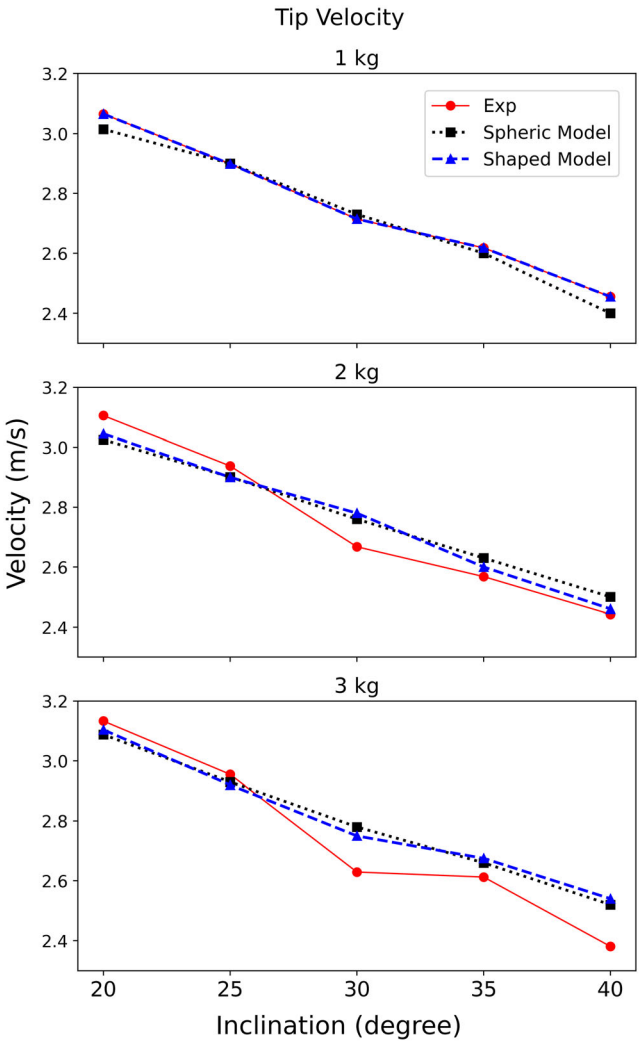

Figure 8. Comparison between the exit velocities of compacted steel scrap particles as they have been determined experimentally and by DEM simulations using both modeling scenarios.

Therefore, the model describing the flow of particles along and from the inclined chute has been set up using only the experimental data concerning the compacted type of steel scrap assuming that the flowing behavior of the different steel scrap shapes is similar to each other. For the modeling of the compacted scrap flow, two approaches were attempted. In the first one, the compacted scrap particles were considered spherical and in the second the effect of their actual shape was taken into consideration.

In **Figure 6**, a comparison between snapshots acquired from the actual flow of a 1 kg batch of steel scrap particles (top) and the corresponding frames of the DEM simulation of the same flow using spherical particles is presented. Clearly, the simulated and experimental flows are very similar to each other. With that as a given, the same comparison was also attempted for different batch sizes and inclination angles.

Figure 7 depicts the fractions of particles collected in the different compartments of the sampling box at different angles of inclination as they have been determined by both simulation scenarios along with those observed during the experimental trials. The simulated predictions are in good agreement with each other and the experimental measurements. However, there are still some discrepancies for some inclinations, more specifically inclinations 25°, 35°, and 40°.

This mismatch is more pronounced for inclination 25° and for larger batches tested at this specific angle, although both the simulated distributions remain in good agreement with each other,

The main reason for these discrepancies stems from possible errors in experimental measurements techniques and also problems related to the sampling box material and position.

As already mentioned in Section 3.1, in the case with an inclination of 25°, the particles of the tested batches fall right onto the upper edge of the wall separating the second from the third compartment of the sampling device. As the size of the tested batch increases, this collision results in a notable wall bending that expands the width of compartment 2 and leads to a higher number of particles being concentrated in the particular compartment. However, this bending and deformation phenomena occurring to the walls of the sampling device as particles collide with them are not considered by the model, and thus the discrepancies between the experimental and simulated mass fractions are observed. This phenomenon might also happen in other cases, however, based on the video analysis, the effect is minor and does not affect the rest of the cases studied since, in all of them, the particles appear to collide with the walls only after they have entered the corresponding compartments, without affecting the upper edge position of theirs and thereupon, the mass fractions of particles collected in the different compartments of the sampling box. Nerveless this phenomenon can still affect the experimental results and collected mass fraction, especially for higher inclination.

The other reason for the mismatch between the measured and modeled mass fraction is the position of the sampling box. In all performed experiments, for a fixed inclination, it has been tried to fix the sampling box in place and the same exact position. However, this positioning is still not precise and the sampling box can slightly deviate from the original position while preparing it for the experiment and also during the experiments when particles are falling into the sampling box and hitting the walls. According to observations during the experimental campaign, even the slightest change in sampling box position for a fixed inclination could change the fate of particles ending up in different compartments causing slightly different mass fractions in slots.

The problem with wall bending and also sampling box fixation is not the case in simulations and the position of included geometries can be precisely fixed and all walls can be considered rigid.

As already mentioned, the velocity of the flow at the tip of the chute is a significant factor determining their trajectory after leaving it and the impact point on the molten bath surface of the furnace. **Figure 8** illustrates the comparison between the average exit velocity of the flows as they have been determined experimentally and by both scenarios of simulation. From the graphs, it is clear that there is a great proximity between the three values for every batch size investigated and every angle of inclination tested. A slight discrepancy between experiments and simulations is observed for the batch size of 3 kg which is more

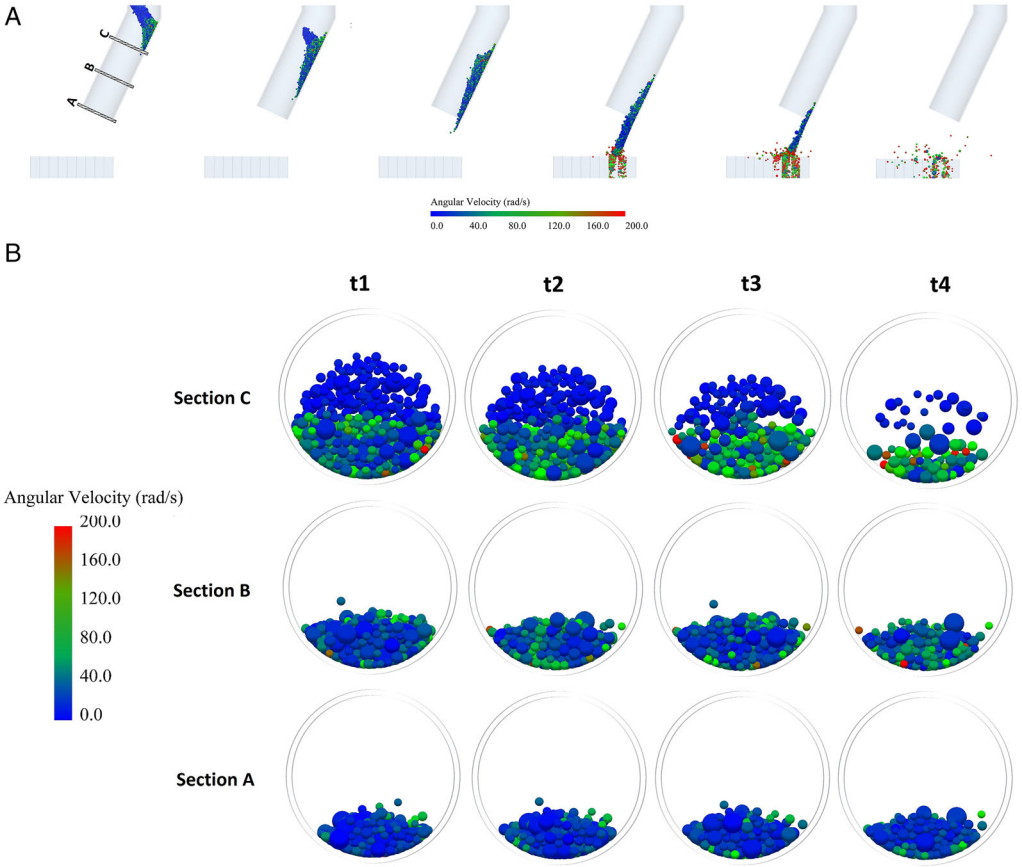

Figure 9. Simulated angular velocity distribution of 3 kg batch particles as they flow in the chute at $\alpha = 25^\circ$ (A: side view, B: cross-section).

noticeable for higher inclinations. In all model predictions, the velocity is decreased linearly for higher inclination. The same trend is measured from the experiments for a batch size of 1 and 2 kg however, for the case of a 3 kg batch, the measured tip velocity from the experiments is not decreased in a linear trend. A slight nonlinearity is also observed for the case of 2 kg but is not as pronounced as in the case of 3 kg. The same nonlinear reduction in tip velocity for higher inclination is reported in the experimental measurements of Yu and Saxen.,[14] but a linear trend by their developed model.

This nonlinearity could be attributed to the experimental measurement errors. As the batch size is increased, the number of particles is increased drastically and a higher number of smaller particles will be included in the flow. This will make the velocity measurements complicated and would induce more errors as particle tracking becomes more harder.

Nevertheless, the predictions for all cases are still within the average error of 10% which was previously discussed in Section 3.1 and depicted in Figure 4.

Moreover, the predictions for spheric and shaped approaches indicate that in the case of compacted steel scrap, the particles' shape factor does not appear to have a significant impact on either the exit velocity or the mass fraction distribution of the particles. Also, the batch size does not appear to affect the exit velocity of the flow. In contrast, the average velocity of the flow at the tip of the chute appears to be strongly influenced by the inclination angle with the exit velocity being almost linearly increased with increasing angles of inclination.

3.3. Velocity Distribution Along the Chute

In this section, the flowing behavior of the steel scrap particles as they propagate along the chute will be analyzed. **Figure 9** shows the modeled particles colored by angular velocity distribution for the inclination of 25° and for 3 kg batch at different cross-sections for different simulation times (t1 to t4 for cross-sectional view). As it can be seen, particles acquire higher angular velocity once hitting the chute wall (where the particles collide with the bottom surface of the inclined part of the chute) and sampling box. In contrast, as the material flows along the chute only individual particles appear to display noticeable angular velocities. In general, the angular velocity of the examined particles is higher at the beginning of the flow when they hit the chute surface (cross-section C) and gets drastically decreased as they flow down the chute (middle cross-section: B and tip cross-section: A).

Figure 10 shows the angular velocity profile for 1 kg batch particles in y-direction and for different cross-sections and angles

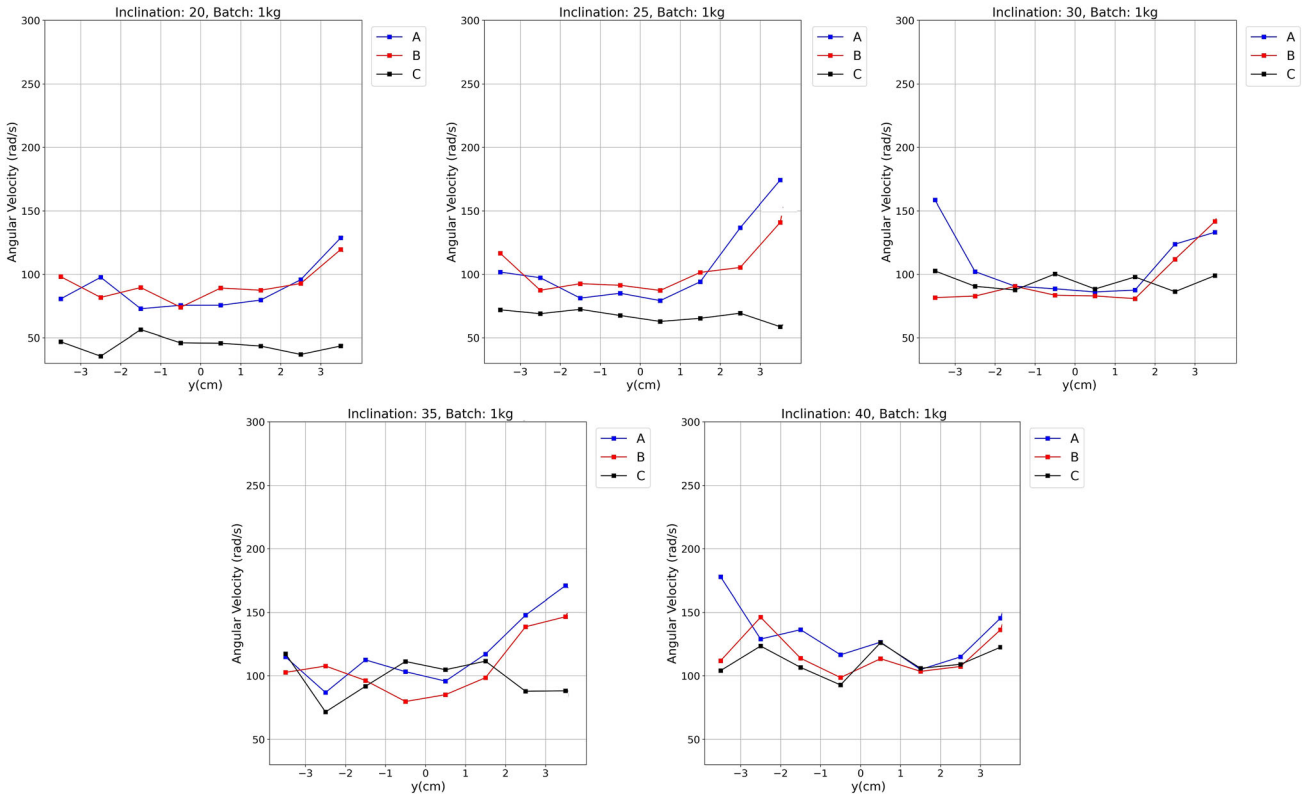

Figure 10. Simulated angular velocity distribution of 1 kg batch particles along y-direction of the chute at different inclination angles and cross-sections.

of inclinations. Each point is calculated as a mean value of the angular velocity of the particles in each y interval. As it can be seen, the mean angular velocity profile is in a V-shaped form with a lower value for particles in the middle of the flow ($y = 0$) than for particles flowing on the sides of the chute. Closer distribution is observed and, in general, an increase in angular velocities is predicted for higher chute angle.

The distribution of the average angular velocity of different batch sizes at different locations of the chute and at 20° and 40° of inclination in the direction perpendicular to the chute is depicted in **Figure 11**. It is clear that at 20° of inclination and regardless of the batch size tested, the particles appear to have the same low angular velocity at the center line and on the sides of the chute. In general, at this low angle of inclination, the particles appear to almost freely flow towards the endpoint of the chute displaying a very limited number of collisions with the chute surface. Therefore, low angular velocities are expected. At 40° of inclination, the angular velocities observed are remarkably higher compared to those at 20° of inclination. In general, the angular velocities are further diminished as the batch size increases and as the flow approaches the exit point of the chute, where only collisions between the flowing particles take place.

In **Figure 12**, the translational velocity of the particles as they flow down the chute is shown. It is clear that when particles collide with the chute (cross-section C) right after the opening of the valve, they decelerate considerably and their translational velocity is remarkably decreased, displaying the exact opposite behavior to that of the angular velocity at the same part of the flow. After this collision, the translational velocity of the particles gradually increases as they flow down the inclined chute to reach a maximum value when they leave the chute tip. However, notable differences in the translational velocity of the flowing particles can still be observed while the materials flow down the chute (cross-section B) and only close to the chute tip (cross-section A) they display an almost uniform velocity distribution.

The translational velocity profile of the 1 kg batch particles at the different cross-sections and inclination angles are presented in **Figure 13**. It is observed that the average translational velocity of the particles appears to have a uniform distribution in y-direction of different cross-sections and at the lower inclination investigated angles, i.e., 20° and 25°. The velocity distribution form is V-shaped at the rest of the chute angles tested with the particles' velocities being slightly higher at the bottom center line than at the sides of the chute. Moreover, a lower mean translational velocity is observed for higher inclination.

As already described, the velocity of the particles at the exit point of the chute (cross-section A) is higher compared to that right after the collision of the particles with the bottom surface of the inclined part of the chute (cross-section A) and that while flowing down the chute (cross-section B). It is also observed that as the inclination angle increases the translational velocity of the particles at every cross-section of the chute investigated notably decreases. Based on the simulated results, it could also be concluded that at the lower inclination angles tested, i.e., 20° and

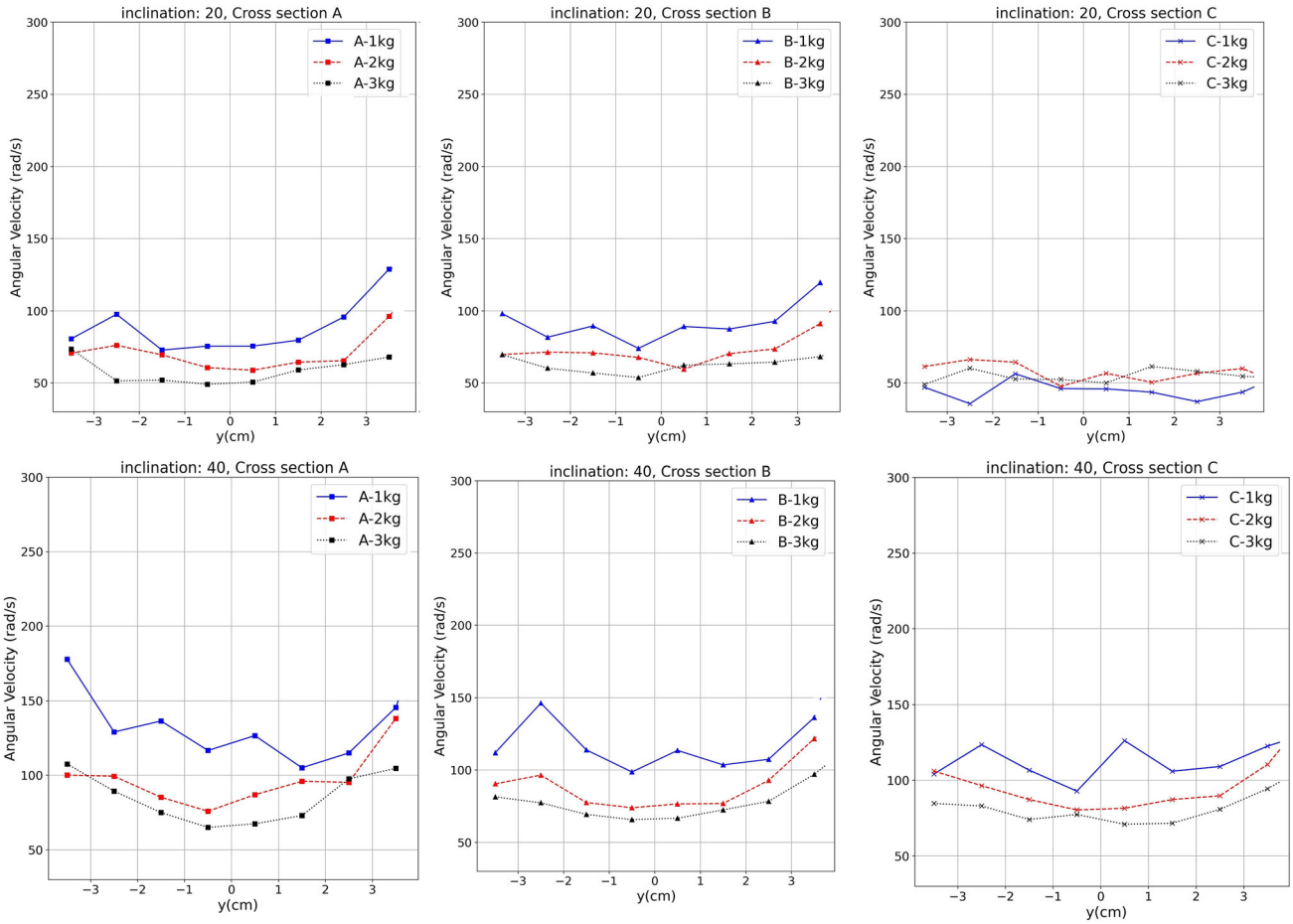

Figure 11. Simulated angular velocity distribution of different batch sizes at 20° and 40° of inclination, as it has been simulated by DEM using spherical particles.

25°, the average translational velocity of the particles appears to have a uniform distribution across the different cross-sections investigated. The velocity profiles of the flowing particles only appear to develop a V-shaped distribution across the different cross-sections

In **Figure 14**, the distribution of the translational velocity of the particles of different batch sizes as they flow down the chute that is positioned at 20° and 40° of inclination is presented. According to the results, as in the case of the angular velocity, at 20°, the average translational velocity of the flow at each of the cross-sections studied is similar regardless of the batch size investigated. Moreover, the particles appear to have the same translational velocity at the center of the chute and at the sides of it. At 40° of inclination, the translational velocities observed are notably lower compared to those observed at 20°. As in the case of the angular velocity, the translational velocity also displays a V-shaped distribution with the velocities at the center line of the chute being lower than those at the sides of it. In addition, the batch size does not seem to have a clear effect on the translational velocity of the flowing particles.

Finally, the effect of the shape of the particles on the distribution of the angular and translational velocity along the different cross-sections has also been investigated. The translational and angular velocity profiles of the different types of flows at each cross-section for both simulation scenarios (i.e., spherical and actual shape) are presented in **Figure 15**. From the graphs, it is clear that the translational velocity profiles, as they have been calculated in the simulation scenario where the effect of the actual shapes of the investigated particles is taken into consideration, follow the same trend as in the spherical particles approach and no notable differences are detected. In contrast, the angular velocities of the two approaches appear to differ from each other. In particular, the angular velocities attributed to the spherical particles are notably higher than the angular velocities calculated in the simulation approach where the effect of the actual shape of the particles is taken into consideration. This should be expected since spherical particles are capable of rotating at a higher velocity compared to irregularly shaped particles. This is in agreement with the findings of Yu and Saxen,[32] who also studied the effect of shape on the translational and angular velocity of pellets and coke and found that only in the angular velocity profiles there is a notable difference between the spherical and actual particles. Nevertheless, they have reported higher angular velocities that the ones that have been found in the current study. However,

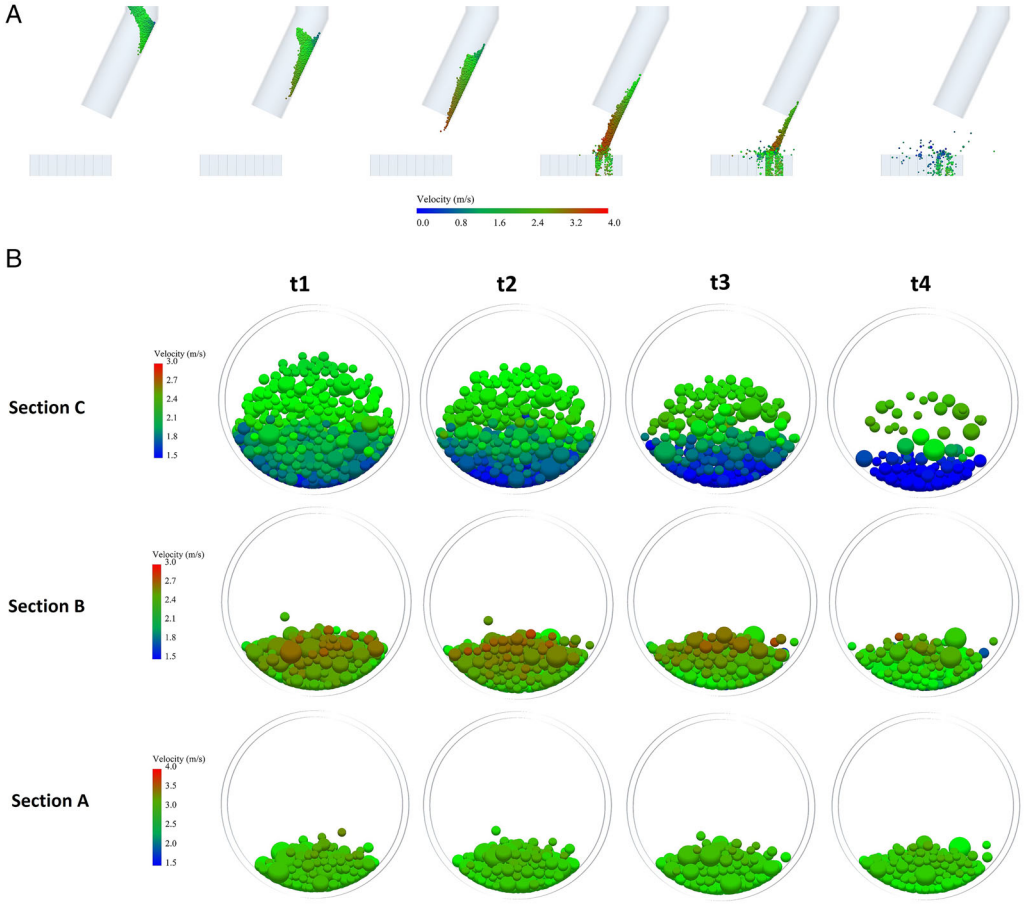

Figure 12. Simulated translational velocity of the 3 kg batch particles as they flow in the chute at $\alpha = 25^{\circ}$ (A: side view, B: cross-section).

this may be due to the different types of material that have been investigated in each study. Moreover, the different modes of feeding that are batch wise in this study and continuous in the one of Yu and Saxen[32] could also be a reason. Conclusively, it could be inferred that the shape, the size, and the properties of the material, as well as the type of feeding mode (batch or continuous) notably, affect the angular velocity of the flowing particles.

4. Conclusions

In this study, an experimental and numerical study of the scrap particle flow was performed. Small-scale experiments were used to investigate the flow of steel scrap particles of different shapes and sizes down an inclined chute with the same dimensions as those of the dosing chute of HIsarna. The main goals of this work were to develop and validate a DEM model using the data obtained from experimental trials and to investigate the cross-sectional distribution of the particles' translational and angular velocity as they flow down the chute. According to the experimental findings, the shape of the steel scrap particles does not influence the exit velocity or the trajectory of the material after leaving the chute. As a result, the model was developed using only the experimental data concerning the compacted type of steel scrap assuming that the flowing behavior of the different steel scrap shapes is similar to each other. By comparing the computational results with the experimental data, it was concluded that the developed model could predict the main features of the investigated granular flow. The study also demonstrated that the average velocity of the particles at the chute tip gradually decreases as the mass of the particles in the chute decreases. This velocity gradient at the chute tip becomes more apparent as the size of the tested batch increases. The angular velocity distribution along the cross-chute direction is V-shaped, whereas the translational velocity displays a more uniform distribution across the y-direction of the chute. As the particles flow down the inclined chute, the angular velocity of the particles decreases, while the translational velocity increases. Nevertheless, both angular and translational velocities become more uniform as the flow reaches the chute tip. Finally, it could be inferred that the model developed in this study can be effectively used to

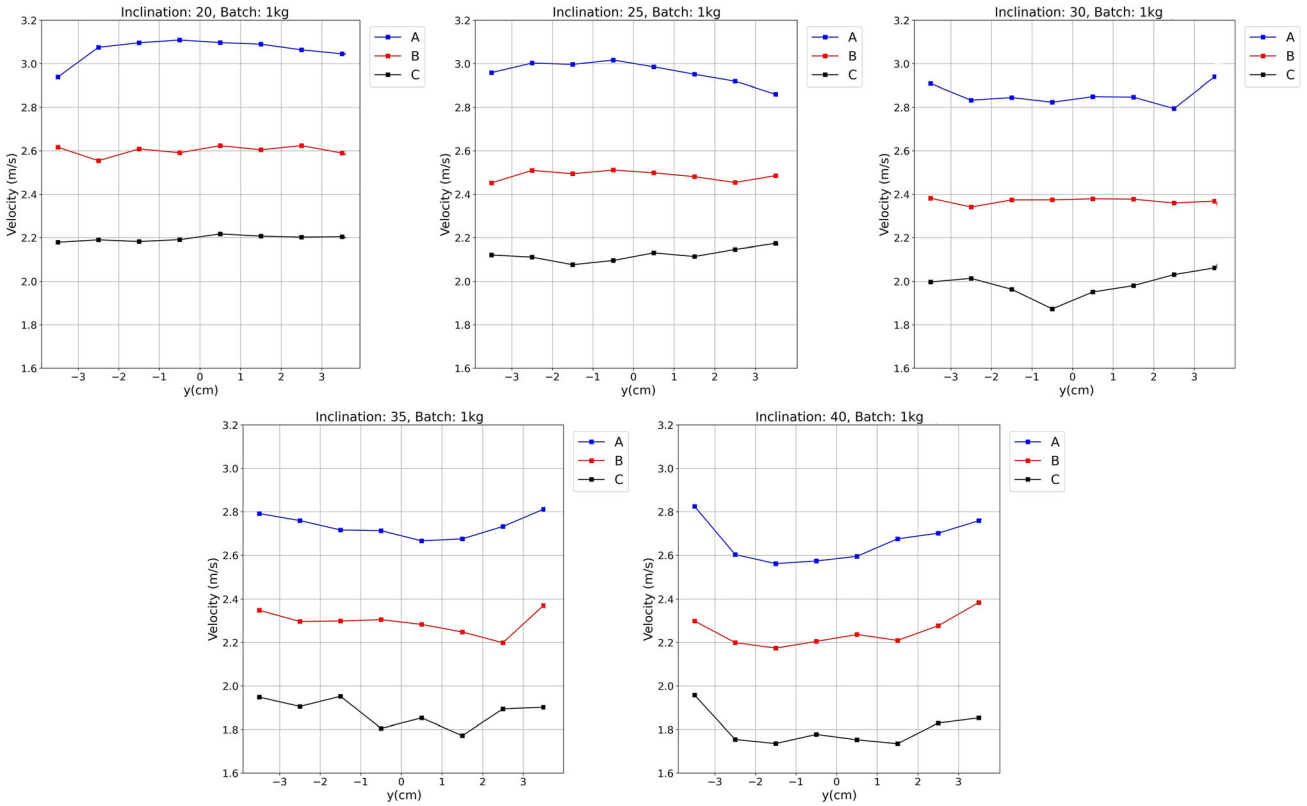

Figure 13. Simulated translational velocity distribution of 1 kg batch particles along y-direction of the chute at different inclination angles and cross-sections.

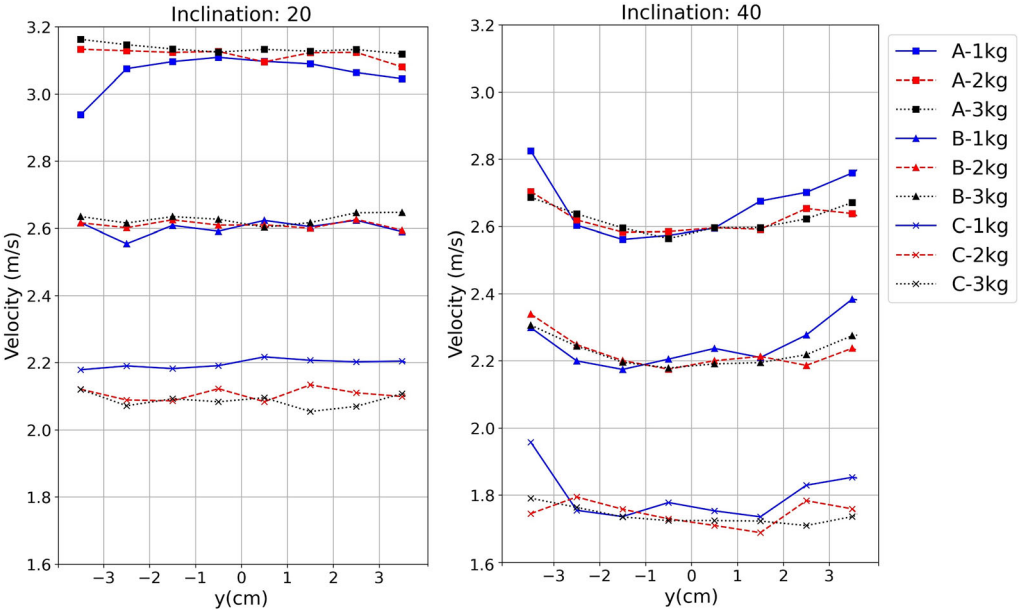

Figure 14. Simulated translational velocity distribution of different batch sizes of particles at 20° and 40°, as it has been calculated by DEM simulations using spherical particles.

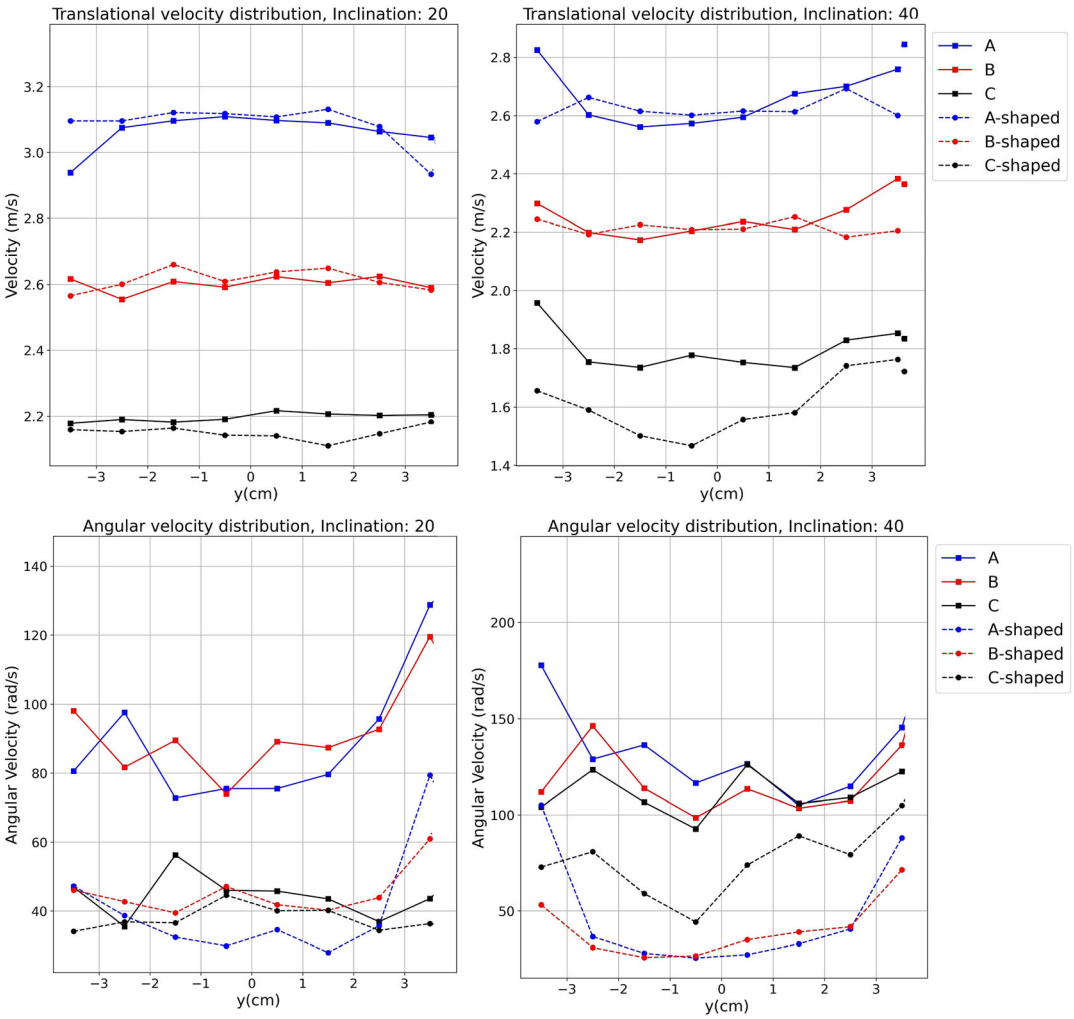

Figure 15. Comparison of the translational (top) and angular velocity (bottom) profiles as they have been determined by the spherical and actual shape (shaped) simulation approaches for a batch size of 1 kg.

forecast particles flowing behavior along and after the chute, as well as their distribution and spreading on the liquid slag surface of the actual plant of HIsarna.

Acknowledgements

The authors would like to thank EIT RawMaterials for funding the Reclamet-project (Nr 17209).

Conflict of Interest

The authors declare no conflict of interest.

Data Availability Statement

The data that support the findings of this study are available on request from the corresponding author. The data are not publicly available due to privacy or ethical restrictions.

Keywords

discrete element methods, granular flow, HIsarna Ironmaking, steel scrap chute, steel scrap flowability

Received: January 26, 2022
Revised: March 10, 2022
Published online: April 4, 2022

[1] M. Barbolini, A. Biancardi, L. Natale, M. Pagliardi, *Cold Reg. Sci. Technol.* **2005**, *43*, 49.
[2] S. P. Pudasaini, K. Hutter, S. S. Hsiau, S. C. Tai, Y. Wang, R. Katzenbach, *Phys. Fluids* **2007**, *19*, 53302.
[3] A. Upadhyay, A. Kumar, A. Chaudhary, *Ann. Glaciol.* **2010**, *51*, 139.
[4] Z. Qing-Zhao, P. Qing, C. Ying, L. Ze-Jun, S. Zhen-Ming, Z. Yuan-Yuan, *Heliyon* **2019**, *5*, e02463.
[5] C. Zhao, L. Jiang, X. Lu, X. Xiao, *Water* **2019**, *11*, 2399.
[6] O. Rufai, Y. C. Jin, Y. C. Tai, *Granular Matter* **2019**, *21*, 62.
[7] D. A. Augenstein, R. Hogg, *Powder Technol.* **1974**, *10*, 43.
[8] M. Ishida, T. Shirai, *J. Chem. Eng. Jpn.* **1979**, *12*, 46.
[9] R. Gudhe, K. R. Rajagopal, M. Massoudi, *Acta Mech.* **1994**, *103*, 63.

[10] O. Pouliquen, N. Renaut, *J. Phys. II* **1996**, *6*, 923.
[11] O. Pouliquen, *Phys. Fluids* **1999**, *11*, 542.
[12] L. E. Silbert, J. W. Landry, G. S. Grest, *Phys. Fluids* **2003**, *15*, 1.
[13] P. G. Rognon, J. N. Roux, M. Naaïm, F. Chevoir, *Phys. Fluids* **2007**, *19*, 58101.
[14] Y. W. Yu, H. Saxén, *Ironmaking Steelmaking* **2011**, *38*, 432.
[15] P. Jop, Y. Forterre, O. Pouliquen, *Nature* **2006**, *441*, 727.
[16] W. Bi, R. Delannay, P. Richard, A. Valance, *Phys. Fluids* **2006**, *18*, 123302.
[17] S. S. Shirsath, J. T. Padding, N. G. Deen, H. J. H. Clercx, J. A. M. Kuipers, *Powder Technol.* **2013**, *246*, 235.
[18] W. Peng, Y. He, T. Wang, *Adv. Powder Technol.* **2014**, *25*, 896.
[19] H. A. Khawaja, *J. Comput. Multiphase Flows* **2015**, *7*, 227.
[20] L. Zhou, L. Zhang, L. Bai, W. Shi, W. Li, C. Wang, R. Agarwal, *RSC Adv.* **2017**, *7*, 12764.
[21] R. K. Soni, R. Mohanty, S. Mohanty, B. K. Mishra, *Adv. Powder Technol.* **2016**, *27*, 531.
[22] Y. Xu, C. Xu, Z. Zhou, J. Du, D. Hu, *Particuology* **2010**, *8*, 141.
[23] P. W. Cleary, M. L. Sawley, *Appl. Math. Modell.* **2002**, *26*, 89.
[24] A. Anand, J. S. Curtis, C. R. Wassgren, B. C. Hancock, W. R. Ketterhagen, *Chem. Eng. Sci.* **2008**, *63*, 5821.
[25] J. Qiu, D. Ju, J. Zhang, Y. Xu, *Powder Technol.* **2017**, *314*, 218.
[26] H. Tangri, Y. Guo, J. S. Curtis, *Chem. Eng. Sci.: X* **2019**, *4*, 100040.
[27] G. Degrassi, L. Parussini, M. Boscolo, N. Petronelli, V. Dimastromatteo, *SN Appl. Sci.* **2021**, *3*, 242.
[28] S. S. Shirsath, J. T. Padding, H. J. H. Clercx, and J. A. M. Kuipers, in *Procedia Engineering*, Vol. *102*, Elsevier Ltd, **2015**, pp. 731–40.
[29] C. Y. Kuo, L. T. Sheng, S. Y. Chiu, Y. Z. Yang, Y. C. Tai, S. S. Hsiau, *Phys. Fluids* **2015**, *27*, 13305.
[30] S. S. Shirsath, J. T. Padding, J. A. Kuipers, T. W. Peeters, H. J. H. Clercx, *AIChE J.* **2014**, *60*, 3424.
[31] H. Mio, S. Komatsuki, M. Akashi, A. Shimosaka, Y. Shirakawa, J. Hidaka, M. Kadowaki, S. Matsuzaki, K. Kunitomo, *ISIJ Int.* **2008**, *48*, 1696.
[32] Y. Yu, H. Saxén, *Ind. Eng. Chem. Res.* **2012**, *51*, 7383.
[33] DEM Solutions Ltd, *EDEM 2.6 Theory Reference Guide*. Copyright 2014, **2004**.
[34] J. Horabik, M. Molenda, *Biosyst. Eng.* **2016**, *147*, 206.
[35] C. Thornton, Z. Ning, *Powder Technol.* **1998**, *99*, 154.
[36] P. Parafiniuk, M. Molenda, J. Horabik, *Comput. Electron. Agric.* **2013**, *97*, 40.
[37] J. P. K. Seville, C. D. Willett, P. C. Knight, *Powder Technol.* **2000**, *113*, 261.
[38] G. Kuwabara, K. Kono, *Jpn. J. Appl. Phys., Part 1* **1987**, *26*, 1230.
[39] H. Kruggel-Emden, E. Simsek, S. Rickelt, S. Wirtz, V. Scherer, *Powder Technol.* **2007**, *171*, 157.
[40] Y. Tsuji, T. Tanaka, T. Ishida, *Powder Technol.* **1992**, *71*, 239.
[41] L. Vu-Quoc, X. Zhang, *Mech. Mater.* **1999**, *31*, 235.
[42] A. B. Stevens, C. M. Hrenya, *Powder Technol.* **2005**, *154*, 99.
[43] A. Anand, J. S. Curtis, C. R. Wassgren, B. C. Hancock, W. R. Ketterhagen, *Chem. Eng. Sci.* **2009**, *64*, 5268.
[44] T. O. Althaus, E. J. Windhab, N. Scheuble, *Powder Technol.* **2012**, *217*, 599.
[45] G. Liu, S. Li, Q. Yao, *Powder Technol.* **2011**, *207*, 215.
[46] C. M. Sorace, M. Y. Louge, M. D. Crozier, V. H. C. Law, *Mech. Res. Commun.* **2009**, *36*, 364.
[47] X. Zhang, L. Vu-Quoc, *Mech. Mater.* **2000**, *32*, 115.
[48] R. D. Mindlin, H. Deresiewicz, *J. Appl. Mech.* **2021**, *20*, 327.
[49] R. Balevičius, Z. Mróz, *Procedia Eng.* **2013**, *57*, 167.
[50] S. T. Nase, W. L. Vargas, A. A. Abatan, J. J. McCarthy, *Powder Technol.* **2001**, *116*, 214.
[51] E. Alizadeh, F. Bertrand, J. Chaouki, *Powder Technol.* **2013**, *237*, 202.
[52] Y. C. Zhou, B. D. Wright, R. Y. Yang, B. H. Xu, A. B. Yu, *Phys. A* **1999**, *269*, 536.
[53] Y. Yu, H. Saxén, *Chem. Eng. Sci.* **2010**, *65*, 5237.
[54] M. Marigo, E. H. Stitt, *Kona Powder Part. J.* **2015**, *32*, 236.
[55] Z. Yan, S. K. Wilkinson, E. H. Stitt, M. Marigo, *Comput. Part. Mech.* **2015**, *2*, 283.